Carbohydrate Polymers 269 (2021) 118335

Contents lists available at ScienceDirect

Carbohydrate Polymers

journal homepage: www.elsevier.com/locate/carbpol

Chemical modification strategies for viscosity-dependent processing of gellan gum

Christine Gering [a,*], Anum Rasheed [a], Janne T. Koivisto [a,b], Jenny Párraga [a], Sampo Tuukkanen [a], Minna Kellomäki [a]

[a] Faculty of Medicine and Health Technology, Tampere University, 33720 Tampere, Finland
[b] Division of Pathology, Department of Laboratory Medicine, Karolinska Institute, 171 77 Stockholm, Sweden

ARTICLE INFO

Keywords:
Hydrogel
Modified gellan gum
Viscoelastic properties
Mechanical testing
Bioprinting

ABSTRACT

Recently, the hydrogel-forming polysaccharide gellan gum (GG) has gained popularity as a versatile biomaterial for tissue engineering purposes. Here, we examine the modification strategies suitable for GG to overcome processing-related limitations. We emphasize the thorough assessment of the viscoelastic and mechanical properties of both precursor solutions and final hydrogels. The investigated modification strategies include purification, oxidation, reductive chain scission, and blending. We correlate polymer flow and hydrogel forming capabilities to viscosity-dependent methods including casting, injection and printing. Native GG and purified NaGG are shear thinning and feasible for printing, being similar in gelation and compression behavior. Oxidized GGox possesses reduced viscosity, higher toughness, and aldehydes as functional groups, while scissored GGsciss has markedly lower molecular weight. To exemplify extrudability, select modification products are printed using an extrusion-based bioprinter utilizing a crosslinker bath. Our robust modification strategies have widened the processing capabilities of GG without affecting its ability to form hydrogels.

1. Introduction

Gellan gum (GG) and its derivatives have been established hydrogel materials suitable for tissue engineering and biomedical sciences (Stevens et al., 2016). Indeed, GG shows high biocompatibility, no cytotoxicity, easy processability, a similar secondary helix structure to collagen, and mechanical properties similar to soft tissue (Oliveira et al., 2010). On the other hand, GG has several limitations, such as a lack of specific cell adhesion sites (da Silva et al., 2014), a precarious gelation temperature for many cell therapy strategies (Gong et al., 2009) as well as high viscosity of precursors. These limitations complicate sterilization by filtration and the formulation of injectable medicines. To fulfill the requirements for tissue engineering, regenerative medicine, and the delivery of biomolecules, hydrogels must gelate under mild conditions. Commonly, it is required for the modification products to retain their ability to crosslink and form hydrogels. We hypothesize that GG can be modified to suit different applications and enable hydrogel formation. Therefore, we propose to modify the chemical and mechanical nature of GG using the inexpensive and gentle strategies: 1) Purification of native GG to lower solution viscosity and facilitate processing. 2) Oxidation of GG to introduce reactive sites for further functionalization and crosslinking strategies. 3) Scissoring to decrease the viscosity and improve syringeability (Fig. 1).

The purification process removes counterions from the commercial GG formulation, reduces the tendency of GG to form gels upon cool down, and decreases the viscosity of the polymer solution (Doner, 1997; Kirchmajer D et al., 2014). Oxidation via Malaprade reaction (Wang, 2010) opens the saccharide ring at the α-L-rhamnose sugar, skews the polymer backbone, and impairs formation of double helices (Morris et al., 2012). We modulate this reaction to retain gel formation capacity while providing reactive sites, namely, the aldehyde groups of oxidized rhamnose. Scissoring, i.e. oxidation and subsequent reduction of the GG polymer chain, restores the original degree of reactivity but decreases molecular weight and viscosity (Gong et al., 2009). After a rigorous analysis of the modified GG in terms of modification degree and composition, we prepare self-supporting hydrogels employing $CaCl_2$ and spermidine (SPD) as crosslinkers (Koivisto et al., 2017). To study the value of aldehyde groups in oxidized GG backbone, we introduce the cationic polysaccharide chitosan. Chitosan has previously been blended with native GG, demonstrating the ability to form electrostatic

* Corresponding author.
E-mail address: christine.gering@tuni.fi (C. Gering).

https://doi.org/10.1016/j.carbpol.2021.118335
Received 17 February 2021; Received in revised form 8 June 2021; Accepted 9 June 2021
Available online 15 June 2021

complexes (Kumar et al., 2016).

This work is the first systematic study of formulations based on modified GG with emphasis on the analysis of precursors and final hydrogels using rheological and compression measurements. Flow curves are prepared to analyze the viscosity of hydrogel precursors and the influence of solvents, and ultimately to provide an insight into extrusion behavior (Paxton et al., 2017). Time sweeps demonstrate the gelation behavior of different formulations, and amplitude sweeps complement viscoelastic characterization of fresh gels. Fully cured gels are subjected to compression testing to assess their mechanical properties. We achieve a standardized hydrogel analysis to identify network formation clues and to assess final mechanical properties resulting from the modifications. Molar mass analysis was performed using size-exclusion chromatography (SEC) coupled with multi-angle light scattering (MALS) detector and the modified compounds were assessed using ^{1}H NMR. To demonstrate the processability of the modified GG and correlate the physicochemical characteristics, we use the materials as ink for extrusion-based printing. Thus, we are proposing an easily adaptable hydrogel platform with tunable mechanical properties and known biocompatibility that suits different needs without altering the underlying material.

2. Materials and methods

2.1. Materials

Gellan gum was purchased from Sigma (Gelzan™ CM-Gelrite®, low acyl form, 1000 kg/mol), and deacetylated chitosan was acquired from NovaMatrix (Protasan UP CL 113, deacetylation degree 75–90%, water-soluble at neutral pH, M_w 50–150 kg/mol, measured as chitosan acetate). Dialysis membrane (Spectra/Por® 12–14 kDa) was purchased from Spectrum Laboratories (Rancho Dominguez, CA, USA). Other chemicals were purchased from Sigma Aldrich and used as received.

2.2. Modifications

Purification of GG is based on the protocol by (Doner, 1997). Briefly, GG was dissolved in water at 0.5% w/v and heated to 60 °C. An excess of cation exchange resin (Dowex, H^+ form, 50–100 mesh, pre-rinsed) was added and separated from the solution after 30 min. The pH was adjusted to 7.5 with NaOH (1 M). The solution was precipitated in isopropanol and the product (NaGG) was lyophilized.

For oxidation of GG, 100 mL GG (0.5% w/v in water) was heated to 40 °C. Under nitrogen atmosphere and in the dark, different amounts of sodium periodate ($NaIO_4$) were dissolved in 4 mL water and added dropwise to the GG solution. Here, we used 12 mg for GGox(1), 24 mg for GGox(2), and 48 mg for GGox(3). The reaction was kept in the dark at 40 °C for 4 h before quenching with ethylene glycol (300 µL). The product (GGox) was dialyzed (12–14 kDa MWCO) over 3 days against water and lyophilized over 4 days.

To scissor, 100 mg of oxidized GG (GGox 1, 2, or 3) was dissolved in sodium borate buffer (46 mL, 0.05 M) under stirring at 60 °C for 1 h. The solution was cooled below 10 °C and kept under nitrogen atmosphere. $NaBH_4$ (4 mL, 1 mg/mL) in sodium borate buffer (0.05 M) was added dropwise to the GGox solution and the solution was stirred overnight. The reaction was quenched by addition of an acetic acid-methanol mixture (5 mL; 1:4) and dialyzed (MWCO 12–14 kDa) against water over 2 days. The product (GGsciss) was lyophilized over 4 days. For nomenclature, scissoring transforms GGox(1) to GGsciss(1) and so forth.

2.3. Hydrogel preparation

GG and its derivates presented herein were dissolved in water (Sartorius, 0.055 µS/cm^3) at 10% w/v, sucrose (10% w/v in water) or

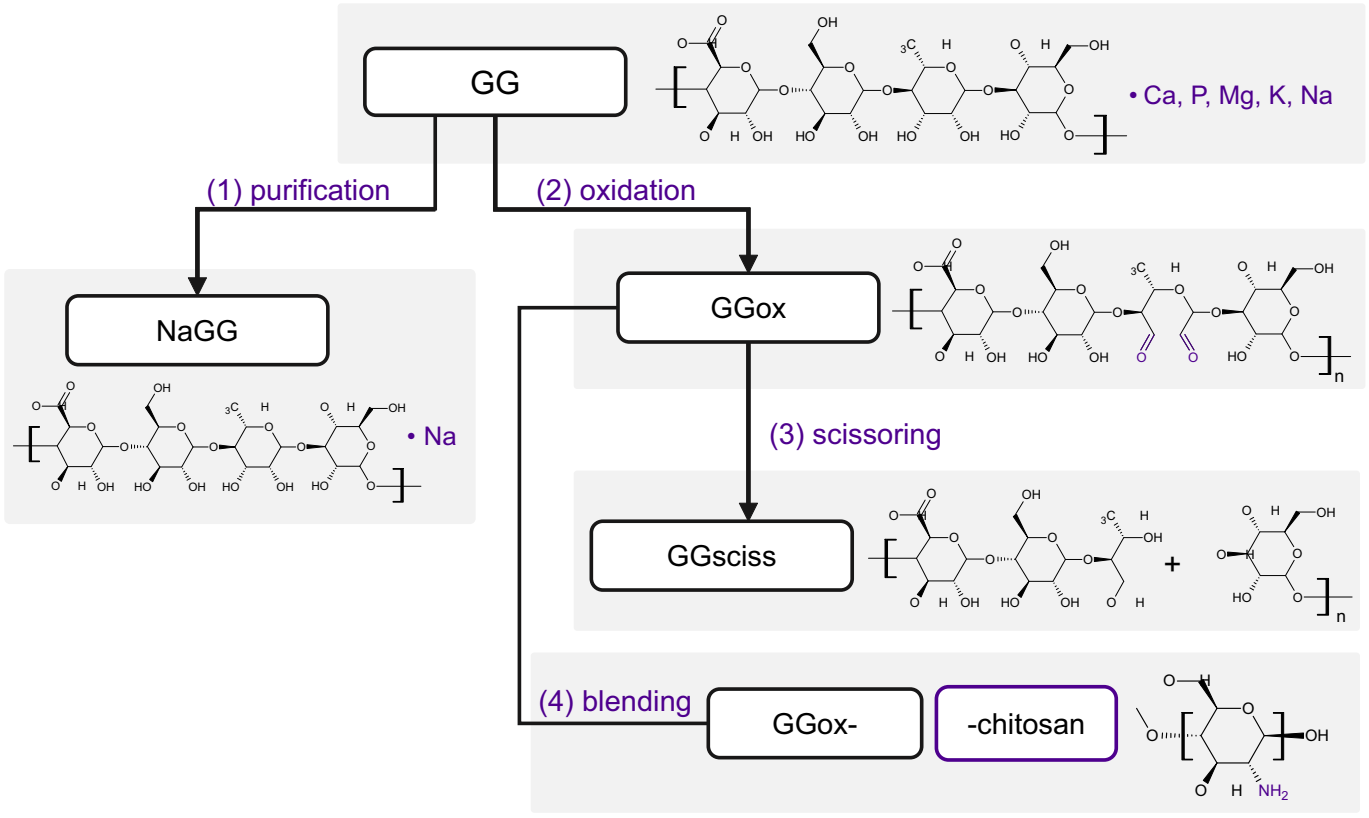

Fig. 1. Chemical structures of native and modified GG (1) Purification creates NaGG. (2) Oxidation creates aldehyde groups in GGox. (3) Subsequent scissoring produces GGsciss. (4) Blending with chitosan uses aldehydes for compounding.

HEPES/sucrose (25 mM, 10% w/v sucrose, pH 6.5), under constant stirring at 50 °C for 1 h. The solutions were stored at 4 °C and warmed to 37 °C before hydrogel preparation.

When casting gels, precursor solutions and crosslinker were mixed in a vial under constant stirring at 37 °C with a fixed volume ratio of 5:1, using either calcium chloride ($CaCl_2 \cdot H_2O$, 5–100 mM) or spermidine trihydrochloride (SPD, 2–20 mM). The hydrogel was then swiftly cast to the mold (Gering et al., 2017).

When blending oxidized GG with chitosan, the chitosan solution (5 mg/mL in HEPES/sucrose at pH 6.5) was added in 1:1 ratio to the crosslinking solution (SPD, 40 mM), and the gels were cast as described above. Essentially, chitosan is treated as component of the crosslinker and the 5:1 volume ratio is maintained for mold-cast hydrogels.

2.4. Analysis methods

Inductively coupled plasma optical emission spectroscopy (Agilent Technologies, 5110 ICP-OES) was used to verify ion concentration for native and purified GG as previously described in (Gering et al., 2019). Briefly, GG was digested in sulfuric acid (H_2SO_4, 98% w/w), cleared with hydrogen peroxide (H_2O_2, 30% w/w), and diluted with water. The solutions were analyzed for Na, Ca, Mg, and K concentrations.

The degree of oxidation was assessed using TBC-TNBS method based on (Bouhadir et al., 1999) with detailed protocol in Appendix D. Briefly, GG and GG derivatives were incubated overnight with an excess of *t*-butyl carbazate (TBC, 10 mM). Picryl sulfonic acid (TNBS, 2.5 mM) was added to each sample, incubated and quenched with hydrochloric acid (HCl, 0.5 M). The solutions were analyzed using UV–Vis-NIR spectrophotometer (Shimadzu UV-3600 Plus, maximum at 342 ± 4 nm, slit width 5 nm).

Molecular weight (M_w) and size of GG was analyzed using Agilent 1260 HPLC pump and autosampler equipped with a multiangle light scattering detector (DAWN, Wyatt Technology) and a refractive index (RI) detector (Optilab). Size separation was performed using 2 PLgel Mixed-C 300 × 7.5 mm columns. The samples were dissolved in the mobile phase (DMSO with 0.2% LiBr) overnight, then heated at 70 °C for 2 h, and filtered (0.45 μm) before injection (100 μL, flow rate 0.5 mL/min).

To record ^{1}H NMR, native and oxidized GG samples were dissolved in D_2O, treated with TBC and stirred at 37 °C for 3 h. After addition of sodium cyanoborohydride the mixture was kept stirring overnight. The product was then analyzed using Jeol 500 MHz equipment without further purification. Chemical shifts: δ 5.15 (s, 1H, CH-1 of rhamnose unit), 4.72 (s, 1H, CH-1 of glucose unit), 4.56 (s, 1H, CH-1 of glucuronic acid unit), 4.07–3.43 (m, 5H, CH-2-5 of units), 1.3 (s, 3H, CH-3 of rhamnose unit).

Rheological measurements were performed using the Discovery HR-2 rheometer and TRIOS software (TA Instruments, USA), which was equipped with a temperature control, using 20 mm plate-plate geometry throughout.

For hydrogel precursor flow comparison, the polymers were dissolved in ultra-pure water, sucrose, or HEPES/sucrose. The solutions were warmed to facilitate the manipulation of the more viscous precursors. A steady state flow shear rate sweep test was performed using 1000 μm gap, with logarithmic sweep, shear rate from 0.01 to 500 s^{-1} (5 points/s) and 25 s sampling period at 25 °C ($n = 3$). To account for wall slip, a stress-controlled flow sweep was carried out, which can be found in Appendix F.

Rheological analysis of the hydrogel formulations, i.e., precursor and crosslinking solution, was performed so that the components were combined on the rheometer plate and the geometry was used for mixing by rapid spinning. The precursor solution was dispensed to the plate at 37 °C, the geometry was lowered to 1500 μm and the crosslinker solution was added during the mixing phase (70 rad/s for 7 s at 37 °C). Consequently, the time sweep started with an amplitude of 0.75% oscillation strain, 0.75 Hz at 30 °C for 30 min ($n \geq 3$). After the sweep had concluded and the gel had formed, an amplitude sweep (30 °C, 0.75 Hz, 0.1–100% oscillation strain, $n = 3$) or frequency sweep (30 °C, 0.75% oscillation strain, 0.1–100 Hz, n = 3) was performed. A solvent trap was used to impede evaporation.

Compression behavior was analyzed using Bose BioDynamic ElectroForce Instrument 5100 and WinTest 8 software (TA Instruments, USA) equipped with 22 N load cell. Cylindrical samples (diameter≈12 mm, height≈4.5 mm, $n = 5$) were tested under uniaxial, unconfined compression in air. The sample was prevented from sliding with wet cellulose paper and compressed with a speed of 10 mm/min to 65% of the original sample height.

2.5. Printing trial

Printability of the hydrogels and the feasibility of a crosslinking bath were tested using Nordson EFD extrusion-based printer (microextruder Nordson EFD E4) and software (DispenseMotion, Nordson, Ohio, USA). The precursor solutions were extruded through a 0.15 mm stainless steel nozzle onto a nylon mesh on a glass substrate. The mesh was soaked in crosslinking solution to ensure an evenly distributed thin layer. The printed structures were in contact with crosslinker for at least 1 min to allow for gelation. The writing speed and the relative humidity were kept constant at 25 mm/s and 55% RH, respectively (Rasheed et al., 2020). Concentrations of precursor solutions and crosslinking baths are presented in Table 2. The photographs were analyzed using ImageJ software (U.S. National Institutes of Health, Bethesda, MD) by measuring the average line thickness and standard deviation of the parallel lines. The printing fidelity is determined as the ratio between standard deviation and average.

3. Results and discussion

We aimed to improve the polysaccharide gellan gum by creating a tunable hydrogel platform for different processing applications, such as extrusion-based printing, mold casting, and injection. The chosen analysis methods reflect their suitability for these different processes, and some of the formulations were printed as a proof-of-concept (see Fig. 7).

Herein, we have investigated two different crosslinking agents, calcium chloride and the bioamine spermidine, to form hydrogels from the modified GG solutions. GG has two complementary gelation mechanisms: first, upon heating and subsequent cooling, the randomly coiled GG chains form highly ordered double helices. Second, the additions of cations link the anionic helices to form a network (Grasdalen & Smidsrød, 1987). Calcium is traditionally used to crosslink a variety of hydrogels including gellan gum. Its hydrodynamic radius and charge density allow ideal intercalation between helical GG molecules. Thus, the crosslinking mechanism is understood to exceed charge screening, as monovalent ions are a weaker crosslinker even at competing charge concentration (Morris et al., 2012). Spermidine is a polyamine found in the ribosome of natural tissues. At pH values below 8.8, it carries three charged amine groups (Wang & Casero, 2006) and is thus able to crosslink the anionic GG as shown by (López-Cebral et al., 2013) and (Koivisto et al., 2017). The concentration of the crosslinking agent and respective GG derivative was chosen to ensure a self-supporting hydrogel was formed (Table 1).

The modification degree of GGox was calculated from the results of the TNBS-TBC assay, as the molar concentration of aldehydes is expected to be equivalent to the amount of consumed TBC. Hence, the percentage of oxidized rhamnose is 2.8% (GGox(1) 0.232 mM), 10.6% (GGox(2), 0.888 mM), and 24.2% (GGox(3), 2.023 mM), respectively. A graphical representation of the results is shown in Appendix D Fig. D1.

A similar TBC-derivatization was performed to detect the presence of aldehyde groups using ^{1}H NMR (Appendix C). The spectra of GGox(1) and GGox(2) show clear difference in the region of δ 1.4 ppm and 1.25 ppm compared to native GG. The presence of a peak at 1.28 ppm (9H, t-

Table 1
Tabulated values from rheology sweeps and compression tests of self-supporting hydrogel formulations. All GG derivatives are used at 1.0% w/v.

Hydrogel formulation		Amplitude sweep				Frequency sweep	Time sweep	Compression test			
		Linear region (oscillation strain %)	G′ storage modulus (Pa)	G″ loss modulus (Pa)	Tan δ	Linear region (Hz)	End of transient phase (min)	Modulus 1 (kPa)	Modulus 2 (kPa)	Fracture strength (kPa)	Fracture strain (mm/mm)
GG	SPD 10 mM	0.0–6.3	71.0 ± 0.9	20.8 ± 0.3	0.29	0.1–1.0	12.5	3.9 ± 2.4	31.8 ± 15.6	5.9 ± 1.8	33.8 ± 2.5
	$CaCl_2$ 5 mM	0.0–3.2	355.2 ± 4.0	21.1 ± 0.5	0.06	0.1–2.0	15.0	3.7 ± 0.7	34.0 ± 8.7	7.0 ± 1.6	37.9 ± 2.1
NaGG	SPD 4 mM	0.0–0.1	362.3 ± 8.0	51.3 ± 2.5	0.14	0.1–1.3	18.3	14.6 ± 7.9	51.0 ± 7.6	8.8 ± 1.3	27.0 ± 1.6
	$CaCl_2$ 10 mM	0.1–0.6	274.7 ± 9.5	33.4 ± 3.8	0.12	0.1–1.3	20.0	3.4 ± 0.6	13.6 ± 2.0	4.2 ± 1.1	41.9 ± 4.0
GGox(1)	SPD 10 mM	0.0–0.8	398.5 ± 4.0	17.5 ± 1.4	0.04	0.1–2.5	15.0	6.7 ± 3.0	83.1 ± 22.2	14.5 ± 1.3	37.2 ± 2.4
	$CaCl_2$ 25 mM	0.1–0.8	577.7 ± 9.3	17.0 ± 4.3	0.03	0.1–2.5	15.0	11.2 ± 2.9	220.7 ± 21.5	42.1 ± 2.3	44.5 ± 0.8
GGox(2)	SPD 20 mM	0.1–7.9	49.9 ± 1.0	0.4 ± 0.0	0.01	0.1–1.6	12.5	1.7 ± 1.6	54.1 ± 9.7	8.6 ± 1.4	48.1 ± 3.8
	$CaCl_2$ 100 mM	0.5–10.0	62.7 ± 1.3	0.7 ± 0.0	0.01	0.1–1.6	15.0	2.2 ± 0.9	123.9 ± 35.1	18.4 ± 4.8	49.8 ± 3.5
GGox(2) + chitosan	SPD 20 mM	0.1–10.0	104.8 ± 2.8	1.8 ± 0.1	0.02	0.1–2.0	15.0	–	–	–	–
	$CaCl_2$ 75 mM	0.1–7.9	43.2 ± 0.4	1.4 ± 0.1	0.03	0.1–1.6	15.0	–	–	–	–
GGsciss(1)	SPD 7.5 mM	0.0–1.0	1606.7 ± 95.2	71.6 ± 18.3	0.05	–	7.5	–	–	–	–
	$CaCl_2$ 25 mM	0.0–2.0	1177.6 ± 6.0	35.7 ± 2.5	0.03	–	15.0	–	–	–	–

Boc) is partially overlapping the peak corresponding to the rhamnose 1.3 ppm (s, 3H, CH-3 of rhamnose unit), thus preventing quantification.

Ion concentration of purified NaGG has previously been determined using ICP-OES. The values show that in the purified product, low concentrations of calcium (0.08% w/w), potassium (0.25% w/w), and magnesium (0.02% w/w) are present, whereas sodium is available as a counterion (2.73% w/w). (Gering et al., 2019).

M_w and size of GG and GGsciss were determined using size exclusion chromatography (SEC) with coupled multi-angle light scattering (MALS) and refractive index (RI) detector. As shown in Fig. 2, GG has a M_w of 326 ± 5 kDa (PDI 1.7), but the scissored product is markedly smaller with GGsciss(1) 53 ± 1 kDa (PDI 2.0) and GGsciss(2) 48 ± 1 kDa (PDI 2.7). The scissored product has a lower M_w, which is in line with the observed lower viscosity profile. In GGsciss(2), a small portion of the weight fraction is 1000 kDa or larger, which could be residual oxidized fragments that were not reduced and scissored. It was not possible to analyze GGox using the same protocol due to presence of aldehydes, which leads to molecular interaction and aggregation of polymer chains, resulting in an apparent higher M_w with smaller size (Appendix E Fig. E2).

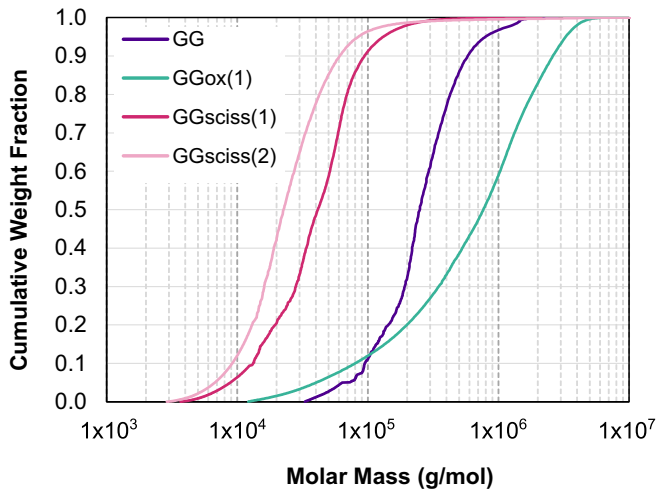

Fig. 2. Cumulative weight fractions of selected GG modifications.

A steady state stress sweep was carried out to produce flow curves of the hydrogel precursors using different solvents with a shear rate from 0.01 to 500 s^{-1}. The resulting curves of viscosity and stress are plotted as double logarithmic plots in Fig. 3.

For native and purified GG, the effect of solvent was investigated using flow sweeps comparing pure water, sucrose solution (10% w/v), and a combination of HEPES buffer (25 mM) and sucrose (10% w/v). Native GG in pure water shows visibly lower viscosity, whereas the HEPES/sucrose had a larger impact on the flow. This effect of sugars has been investigated in detail and can be attributed to molecular crowding and denser association of polymer chains (Morris et al., 2012). Different modification degrees were investigated for oxidation and subsequent scissoring, based on the amount of added reactant. From Fig. 3C and D, we can see that different oxidation degrees have a small effect on viscosity, whereas the effect for scissored GG is negligible. Comparing native and purified GG to oxidized and scissored products, however, shows a significant difference in viscosity profile.

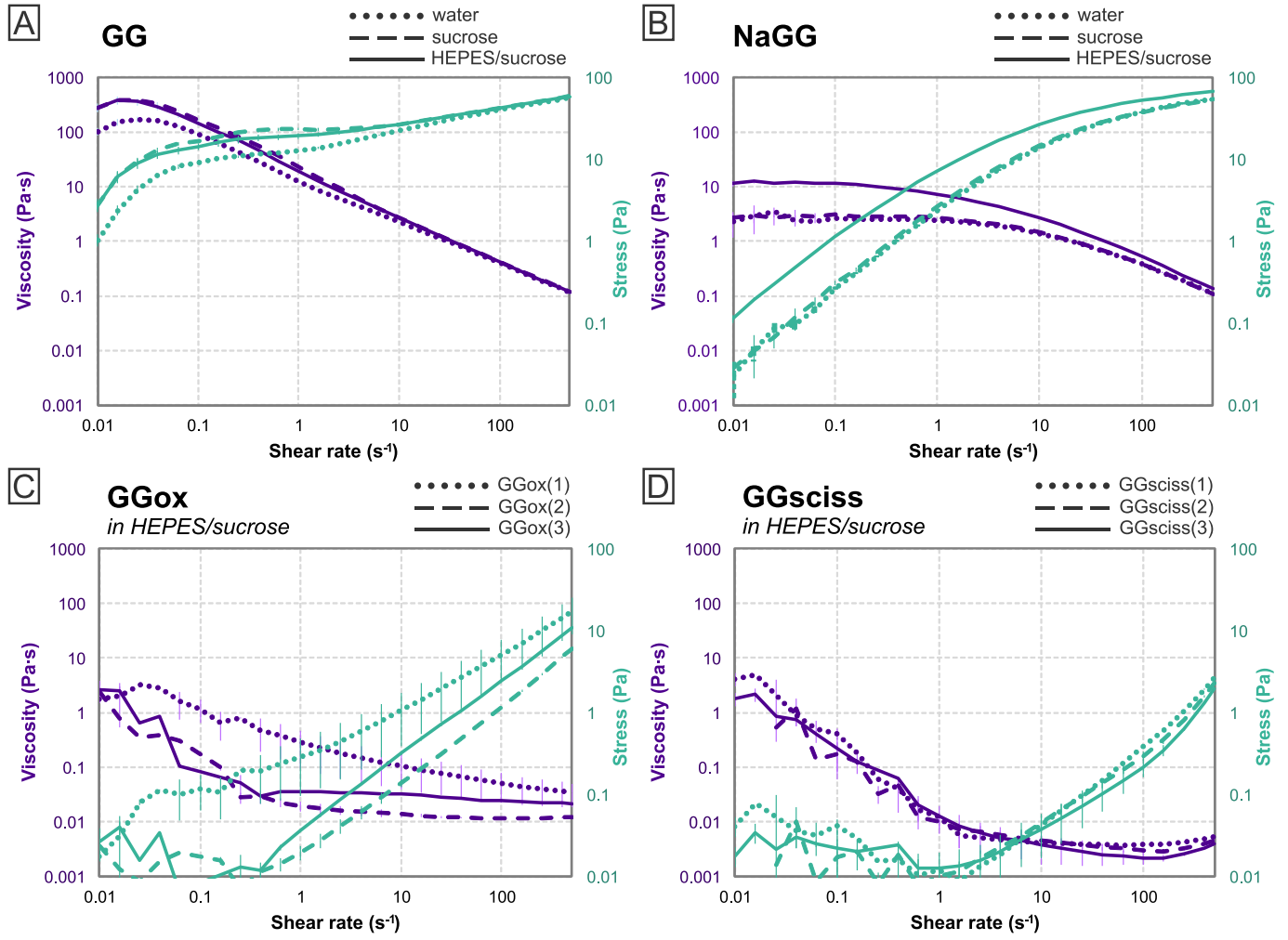

Fig. 3. Flow curves of hydrogel precursor solutions showing viscosity and stress vs. shear rate. A and B) GG and NaGG in different solvents; C and D) GGox and GGsciss with different degrees of modification. ($n = 3$).

From the stress-vs-shear rate plot, the shear behavior of hydrogel precursors can be analyzed. Native GG presents an initial phase of shear thinning behavior with a yield stress range between 1.03 Pa and 2.76 Pa (Fig. 2A). This is followed by more linear behavior above shear rates of 10 s^{-1} as defined by the Bingham model (Chhabra & Richardson, 2008). The curves of purified NaGG (Fig. 3B) clearly show its shear thinning nature, with a low yield stress between 0.02 Pa and 0.11 Pa. The Power Law can be applied for GG above 0.1 s^{-1}, and likely for NaGG above 10 s^{-1}, but not for the other modifications (Appendix G). In contrast, both oxidized GGox and scissored GGsciss (Fig. 3C and D) have near zero yield stress between 0.02 Pa and 0.03 Pa and 0.01 Pa and 0.04 Pa, respectively. Above 1 s^{-1}, GGox is fairly linear, indicating Newtonian fluid behavior, whereas GGsciss shows shear thickening tendency. At low values, measurements become unreliable, and therefore a steady stress sweep should be chosen for low viscosity solutions.

Flow curves are standard evaluation tools when considering polymer solutions for 3D printing applications, and our printing experiment confirmed our findings. Both GG and NaGG demonstrate shear thinning behavior and extruded into repeatable structures with ease. However, GGox is not shear-thinning and both GGox(1) and GGox(2) solutions required higher pressure to extrude. Moreover, due to its extremely low viscosity, GGox(2) showed poor extrudability during printing.

Rheological time sweeps (Fig. 4) provide an excellent tool for studying the network formation of hydrogels by casting the components under the geometry and performing a time sweep with low amplitude and frequency. The gelation sweep is performed so that the precursor is placed between the gap while the geometry itself carries out the mixing by rapidly spinning for a short duration. This assures even contact of the hydrogel with the geometry and prevents internal stresses in the hydrogel. Notably, this allows observation of the early gelation stages and gives an insight into gelation kinetics (Zuidema et al., 2014).

All formulations form self-supporting hydrogels within 30 min of the measurement. The curve, however, does not reach full linearity and a small slope value remains. This indicates that network development continues and justifies longer, e.g., overnight, incubation of samples for mechanical testing of final hydrogels.

Tan δ, the ratio between G′ and G″, gives further indication of the completion of network formation within the gel (Chhabra & Richardson, 2008). Mechanistically, the viscous and elastic components of the hydrogel model are shifting in magnitude related to each other during the transient phase of gelation (Appendix B). Once the gel has set, the value for tan δ should behave linearly (Zuidema et al., 2014). The end of the transient phase marks the time we understand as gelation time; however, the given value (Table 1) is rather qualitative.

The time sweep shows the gelation behavior of each formulation, which is relevant for application techniques, such as mold casting, with a critical time component for handling the hydrogel. Native GG has the highest gelation rate, causing problems for the manipulation of the setting gel components. NaGG, on the other hand, shows very rapid and precarious network formation, with slightly longer time needed to form a stable gel. This may be due to the larger number of crosslinking sites available, as purification deprives the formulation of cations, especially

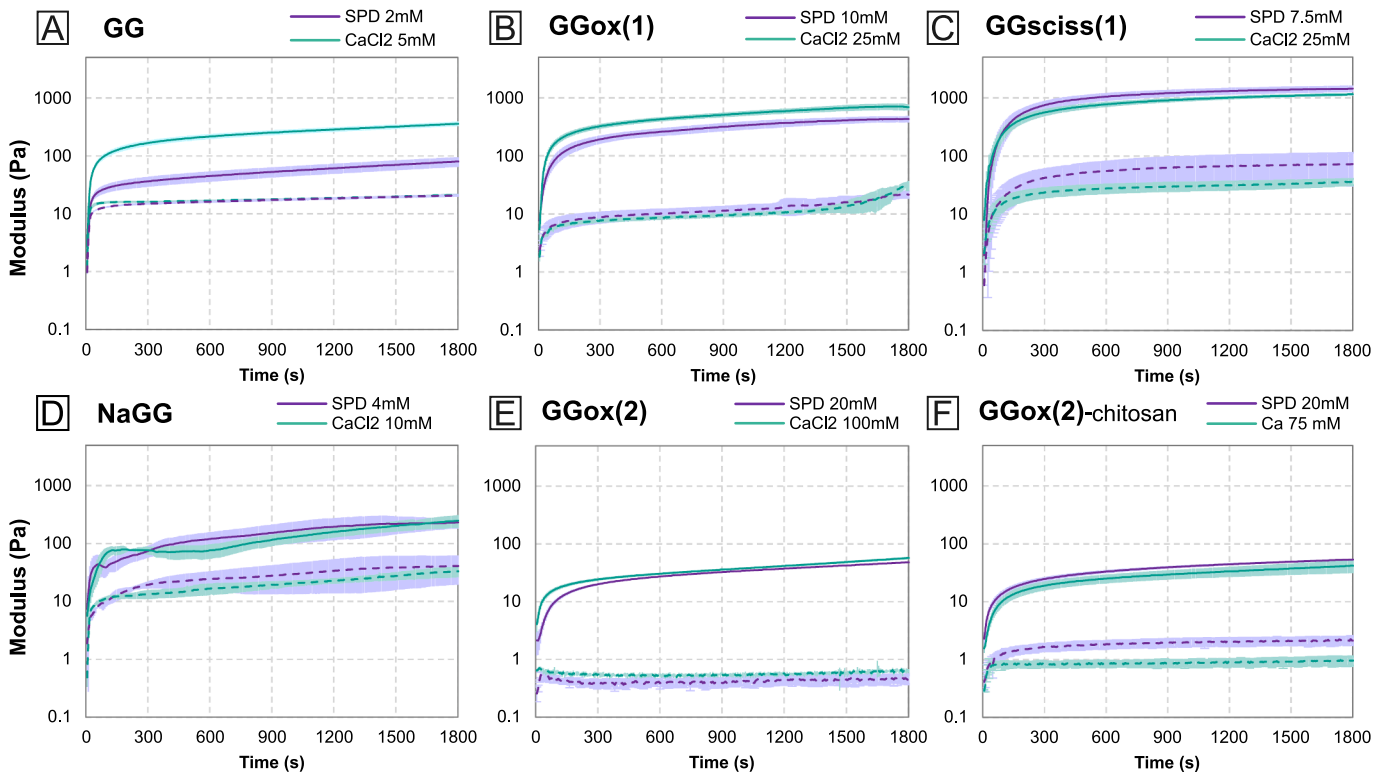

Fig. 4. Time sweeps of hydrogel-forming solutions. Shown are storage G′ (solid line) and loss G" (dashed line) modulus over time with constant amplitude (0.75% osc. strain) and frequency (0.75 Hz). Time point 0 is the end of the mixing phase (7 s) of precursor solution and crosslinker ($n = 3$).

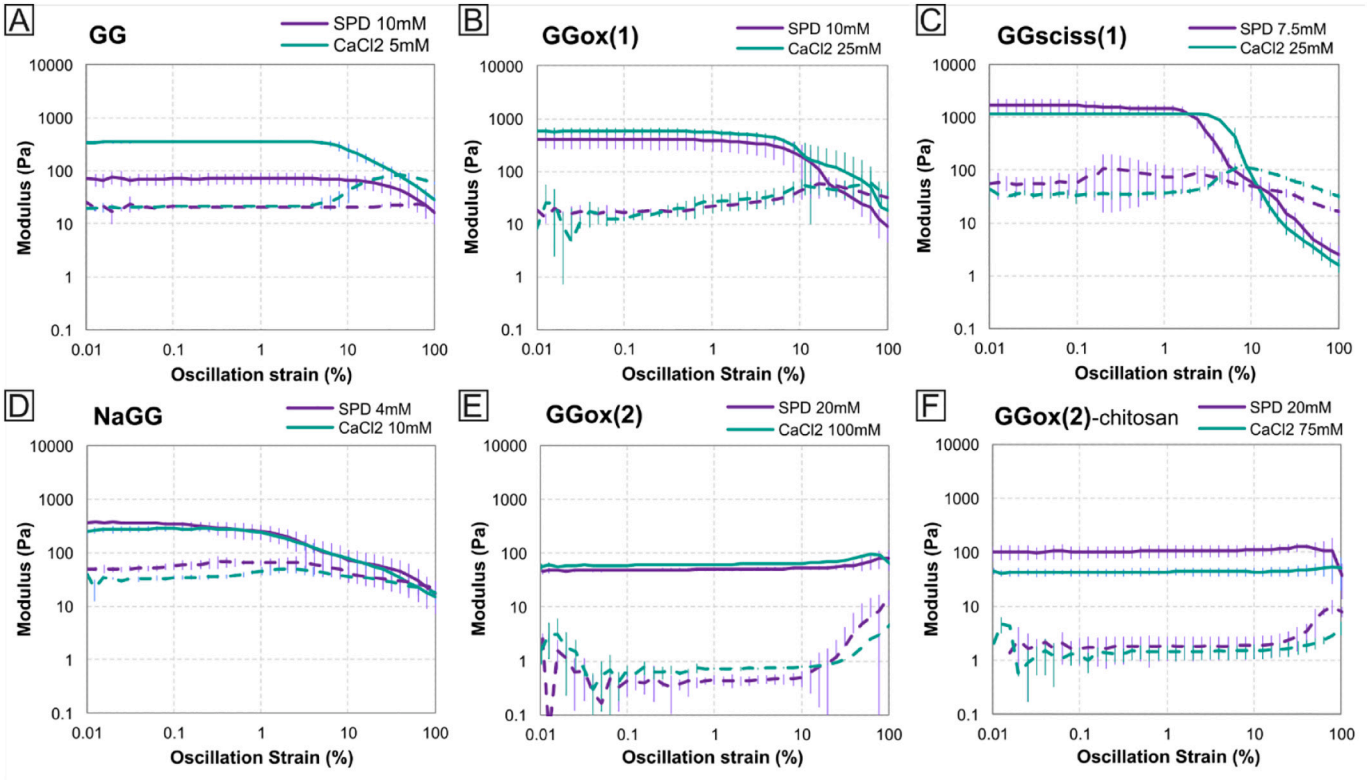

Fig. 5. Amplitude sweeps of different hydrogel formulations. Crosslinker is shown in the upper right hand side of each chart, with storage (solid line) and loss (dashed line) modulus ($n = 3$).

calcium. The oxidized GGox(1) still forms surprisingly tough hydrogels, despite polymer chain distortion, but GGox(2) already struggles to form gels even with higher concentrations of crosslinking agents. Similarly, GGsciss(1) forms gels with calcium and spermidine, but GGsciss(2) does not.

From amplitude sweep measurements we can derive: storage (G′) and loss modulus (G″) at the linear region (SAOS); the range of the linear behavior and its end point, i.e., how much the network deforms before it loses its linearity; behavior type during the non-linear region (LAOS) and in some cases, depending on the measured amplitude range, the crossover point of G″ and G′, which may indicate crosslinking density. The amplitude sweeps shown in Fig. 5 are performed after the time sweep, approximately 30 min after mixing. As previously discussed, the hydrogel at this time point may not be fully formed and is therefore expected to yield different results than a sample that has set overnight.

The linear regions, tan δ as well as G′ and G″, are listed in Table 1. Similar to time sweep, tan δ can be utilized to compare the viscoelastic nature of the formulations. In all hydrogel samples, G′ dominates G″ before the yield point, as they are elastic solids. However, the magnitude of their ratio (tan δ) reveals the extent, with larger values indicating a more associated network. The results of the frequency sweep are presented in SI Appendix A.

In discussing complex fluids, (Hyun et al., 2002) investigated the non-linear region of the amplitude sweep (LAOS) to describe different behaviors linked to the microstructure of the polymer. These behaviors include strain thinning, strain thickening, and strain overshoot phenomena, depending on how the hydrogel reacts to strain. Although we have studied viscoelastic networks rather than fluids, their observations are reflected in the sweeps shown in Fig. 5. For example, regardless of the crosslinker used, GG, NaGG, and GGox(1) all show weak strain overshoot, whereas G" increases before decreasing. This indicates a weakly structured material that experiences large deformation before a critical strain and starting to flow (Hyun et al., 2002). In Fig. 4, this can be clearly seen with GG and $CaCl_2$ as crosslinker. Conversely, GGox(2) and chitosan-containing compounds show strong strain overshoot behavior, where both G′ and G″ increase after the linear region, and before the critical strain destroys the network and both values decrease. Unfortunately, the maximum strain value of 100% oscillation strain does not show full LAOS behavior for all formulations.

Mold cast samples of different formulations were incubated at 37 °C overnight and analyzed using compression. The curves are shown in Fig. 6, whereas moduli and fracture strength are listed in Table 1. Viscoelastic properties are not directly discernable from this type of measurement, as the features of viscoelastic deformation and brittle fracture cannot be separated (Kocen et al., 2017). It is, however, straightforward to compare the fracture behavior between different compositions. Moreover, it is also possible to compare samples of the same composition that have been subjected to different treatments or environments. Therefore, compression testing assesses the static mechanical properties of the final hydrogel, whereas rheology assesses the hydrogel processing kinetics. Ultimately, both techniques work in conjunction to investigate the mechanical properties of hydrogels.

From the compression graph, three features can be assessed: modulus 1, modulus 2, and the fracture point. Modulus 1 describes the presumed elastic region of hydrogel compression. Here, the slope is taken from 1% to 10% compressive strain. Modulus 2 describes the linear region before the fracture point. All GG derivates show a fracture point, indicating their relatively brittle nature. Other hydrogels and native tissue, however, are known to not show a fracture point, dissipating the strain in an elastic manner (Karvinen et al., 2018; Koivisto et al., 2017; Koivisto et al., 2019).

Further, the fracture behavior can be evaluated to compare different

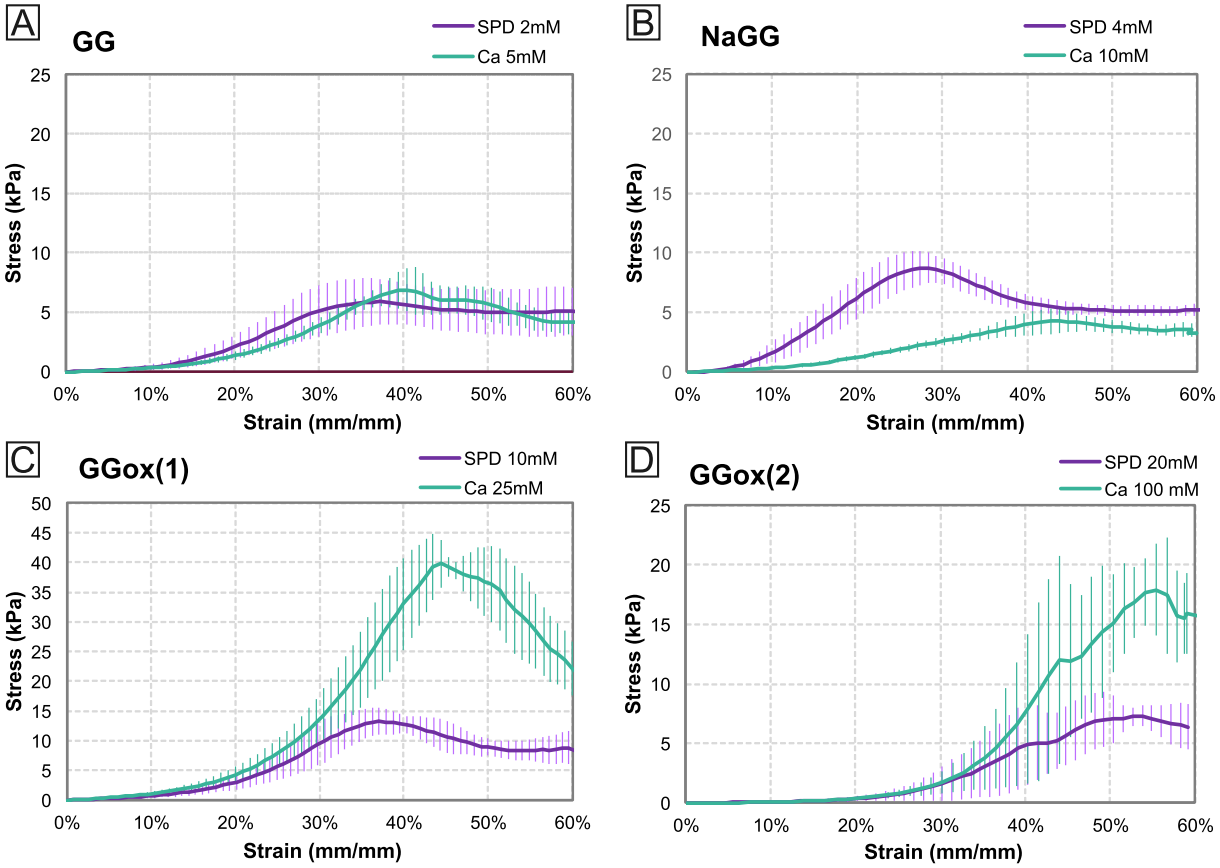

Fig. 6. Stress-strain curves of hydrogel samples under compressive load. Please note different scale of graph C ($n = 5$).

hydrogel formulations, such as the two NaGG-based hydrogels formed with $CaCl_2$ and SPD (Fig. 5B). NaGG-SPD has a steep slope and quick fracture indicating a brittle fracture. In comparison, NaGG-Ca has a shallower slope and higher ductility, which indicates extrusion of water from the surface of the gel and formation of microfractures under the compressive load (Nakamura et al., 2001). Also, GGox(1) and (2) formulated with $CaCl_2$ (25 mM and 100 mM) show very high fracture stress and modulus 2.

From the collected information on mechanical and viscoelastic properties, we can confer the application ranges of different GG modifications. For instance, scissored GG has low viscosity and loses the typical shear-thinning effect of other GG solutions due to the drastic reduction in molar weight seen from the SEC/MALS results. However, GGsciss(1) retains the ability to form self-supporting hydrogels within a short time, with the transient phase ending within 10 min (Appendix B Fig. B1). It is likely the shortened polymer chain and reduced viscosity will help the network find an equilibrium within the crosslinking architecture faster. Whereas dilation rules out printing applications, we suspect the GGsciss polymer precursor may be applicable when syringing for minimally invasive surgery, injecting body-on-chip models, filling cavities, and ophthalmic coatings. Higher degrees of scissoring, such as GGsciss(2) and (3), do not form self-supporting gels, further limiting the application range.

Oxidized GG, on the other hand, can form self-supporting gels with

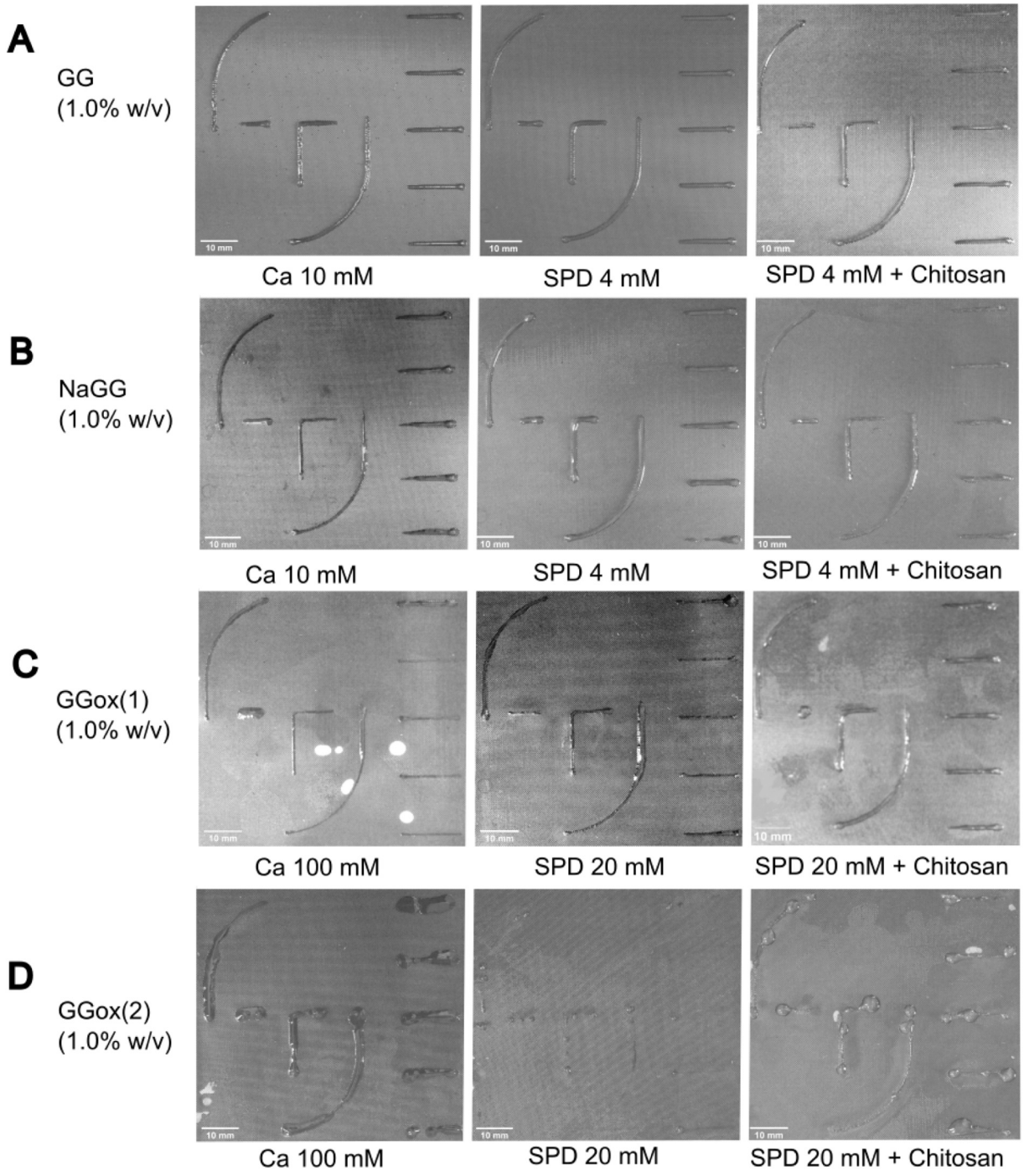

Fig. 7. Photographs of printed structures. The polymer precursor solutions were extruded from a nozzle (stainless steel 0.15 mm) at the shown pressure and constant speed (25 mm/s) onto a treated glass plate with nylon mesh coated in crosslinker solution. Ambient conditions at 20 °C and 56% RH (scale bar 10 mm).

increased crosslinker concentrations. We have demonstrated its ability to be compounded with other substances, such as chitosan, and be expanded for blending with therapeutic agents in drug delivery applications. The active sites of GGox are also beneficial for cell encapsulation, as aldehyde groups are known to be tissue adhesive, whereas native GG is known to be bioinert and does not facilitate cell attachment (Ferris et al., 2013). The oxidation degree can be fine-tuned through iodate concentration in the modification procedure. We have shown previously that a high oxidation degree can be used to compound with modified gelatin to form a chemically crosslinked, self-supporting hydrogel with good cell attachment (Koivisto et al., 2019).

Native GG and purified NaGG are good candidates for printing, which is indicated by the flow test results. Both are shear thinning, although NaGG has a more pronounced viscosity profile and dramatically lower yield stress compared to native GG. Bioprinting is a popular topic in the recent literature (Paxton et al., 2017; Rasheed et al., 2020), and therefore an understanding of hydrogel rheology and mechanical properties before, during, and after such extrusion process is needed. To demonstrate printability, we used extrusion-based bioprinting to print shapes (Fig. 7). To compare the printing behavior, we used other modifications in the trial, although, judging from the results of the flow test, they could have been disregarded. Indeed, the poor printing results are visible from Fig. 7C and D, which supports our conclusions on flow results. To render these polymer solutions suitable for extrusion-based printing, pre-crosslinking with low concentrations of crosslinkers should be considered (Rasheed et al., 2020).

Both GG (1.0% w/v) and NaGG (1.0% w/v) extruded as continuous lines at relatively low pressure (0.90 bar to 0.98 bar). GGox(1) formed a continuous line structure at a higher pneumatic pressure of 1.48 bar, whereas GGox(2) was unable to form unbroken lines at pressures as high as 2.56 bar. This further proves the increased printability of GG and NaGG. This finding is in line with the extrudable hydrogels, such as alginate and gelatin, found in the literature, and verifies that both pressure and viscosity determine printability (He et al., 2016; Paxton et al., 2017).

Table 2 summarizes the average thickness of the five parallel lines, measured from five distinct points, indicating the print fidelity and consistency.

We have shown several facile ways to chemically modify GG, impacting the mechanical and viscoelastic properties. Polymer flow and gelation kinetics are paramount for any extrusion-based processing technique, where bioprinting, casting, and injection have diverse requirements. We have correlated the flow properties and viscosity values to the printing results, while the gelation rheology results will reflect on casting and injection applications. In turn, mechanical stability and behavior of the formed hydrogel will determine the suitability for applications, such as 3D in vitro cell culture, in vivo cell carrier, drug carrier, and phantom material for imaging purposes. Although the mechanical properties of the final hydrogel may not be adequate for printing or self-supporting structures, for example GGox(3) or GGsciss (2), they may be useful in coatings and body-on-chip models. Assessing the syringeability and cavity filling of weak hydrogels, however, requires more sophisticated techniques, and therefore was not performed here.

Table 2
Setup and results of printing trial.

	Polymer	Pressure (mbar)	Crosslinking bath	Line width (mm)	Printing fidelity
A	GG	0.90	$CaCl_2$ 10 mM	1.2 ± 0.1	7.4%
			SPD 4 mM	1.3 ± 0.1	10.2%
			Chitosan 0.5% w/v -SPD 4 mM	0.9 ± 0.1	13.5%
B	NaGG	0.98	$CaCl_2$ 10 mM	1.3 ± 0.3	19.0%
			SPD 4 mM	1.3 ± 0.2	17.1%
			Chitosan 0.5% w/v -SPD 4 mM	1.1 ± 0.2	14.9%
C	GGox (1)	1.48	$CaCl_2$ 100 mM	1.0 ± 0.3	31.4%
			SPD 20 mM	0.8 ± 0.2	17.8%
			Chitosan 0.5% w/v -SPD 20 mM	1.3 ± 0.2	19.1%
D	GGox (2)	2.20–2.56	$CaCl_2$ 100 mM	3.2 ± 0.9	29.5%
			SPD 20 mM	N/A	N/A
			Chitosan 0.5% w/v -SPD 20 mM	1.9 ± 1.0	52.0%

4. Conclusion

We have confirmed our hypothesis by demonstrating suitable modification strategies for GG, resulting in a wide range of precursors which have the capacity to form hydrogels with tunable structure and properties. Modification products can have different applications and uses, depending on flow properties or precursor, and hydrogel mechanical properties. To facilitate the use of the precursors we present their systematic comparison. A significant part of this study was dedicated to the testing of viscoelastic and mechanical properties, alongside discussing the applications of the different derivatization products.

While GG and NaGG both clearly show a shear thinning profile with maximum viscosity values of 383 and 12.4 Pa·s, oxidized and scissored products have much lower viscosity (below 3.2 and 5.0 Pa·s respectively) and do not appear shear thinning. Shear thinning is an essential trait for printability, as highlighted by the good printing fidelity of GG (average 10%) and NaGG (average 17%) compared to the tested GGox modifications (average 23–41%). The SEC-MALS analysis reveals the successful chain scission, as the M_W decreases from 326 kDa (GG) to around 50 kDa for different GGsciss products. From the amplitude and time sweeps, the capacity of different modification products to form hydrogels and their apparent stiffness can be determined. For instance, GGox(1) forms hydrogels with storage modulus between 399 and 578 Pa while GGox(2) is softer with moduli between 50 and 63 Pa. On the other hand, aldehydes of GGox can interact with chitosan and other biomolecules, which can be useful for drug loading or attachment of bioactive factors. GGsciss shows greatly reduced viscosity and molar weight, predicted to be useful for injection-based applications. The results of our study indicate the suitability of GG as hydrogel material platform and our findings establish a basis on which to build a robust material library.

CRediT authorship contribution statement

Christine Gering: Methodology, Validation, Formal analysis, Investigation, Data curation, Writing – original draft, Writing – review & editing, Visualization. **Anum Rasheed:** Methodology, Validation, Formal analysis, Investigation, Data curation, Writing – original draft, Writing – review & editing, Visualization. **Janne T. Koivisto:** Conceptualization, Methodology, Writing – review & editing. **Jenny Párraga:** Conceptualization, Methodology, Validation, Investigation, Writing – original draft, Writing – review & editing, Supervision. **Sampo Tuukkanen:** Resources, Supervision, Funding acquisition. **Minna Kellomäki:** Conceptualization, Resources, Writing – review & editing, Supervision, Project administration, Funding acquisition.

Acknowledgements

This work was supported by the Academy of Finland through the Center of Excellence – Body on Chip (312409, 326587, 336663). C.G. received financial support from the Jenny and Antti Wihuri Foundation

(3a3aec) and A.R. from the TAU Doctoral School. We wish to thank Dr. Vijay Parihar for recording the ^{1}H NMR as well as the Wyatt Technology Corporation for successfully running the SEC and MALS, and Prof Michiel Postema for helpful discussion on rheology assessment.

Appendix A. Supplementary data

Supplementary data to this article can be found online at https://doi.org/10.1016/j.carbpol.2021.118335.

References

Bouhadir K. H., Hausman D. S., & Mooney D. J. (1999). Synthesis of cross-linked poly (aldehyde guluronate) hydrogels. Polymer 40, 3575–3584.

Chhabra, R. P., & Richardson, J. F. (2008). Chapter 2 - Rheometry for non-Newtonian fluids. In R. P. Chhabra, & J. F. Richardson (Eds.), *Non-Newtonian flow and applied rheology* (2nd ed., pp. 56–109). Oxford: Butterworth-Heinemann.

da Silva, L. P., Cerqueira, M. T., Sousa, R. A., Reis, R. L., Correlo, V. M., & Marques, A. P. (2014). Engineering cell-adhesive gellan gum spongy-like hydrogels for regenerative medicine purposes. *Acta Biomaterialia, 10*, 4787–4797.

Doner, L. W. (1997). Rapid purification of commercial gellan gum to highly soluble and gellable monovalent cation salts. *Carbohydrate Polymers, 32*, 245–247.

Ferris, C. J., Gilmore, K. J., Wallace, G. G., & Panhuis, M. I. H. (2013). Modified gellan gum hydrogels for tissue engineering applications. *Soft Matter, 9*, 3705–3711.

Gering, C., Koivisto, J. T., Parraga, J., Leppiniemi, J., Vuornos, K., Hytönen, V. P., … Kellomäki, M. (2019). Design of modular gellan gum hydrogel functionalized with avidin and biotinylated adhesive ligands for cell culture applications. *PLoS One, 14*, Article e0221931.

Gering, C., Koivisto, J. T., Parraga, J. E., & Kellomäki, M. (2017). Reproducible preparation method of hydrogels for cell culture applications – case study with spermidine crosslinked gellan gum. In *Anonymous Embec & Nbc 2017* (pp. 811–814). Singapore: Springer.

Gong, Y., Wang, C., Lai, R. C., Su, K., Zhang, F., & Wang, D. (2009). An improved injectable polysaccharide hydrogel: Modified gellan gum for long-term cartilage regenerationin vitro. *Journal of Materials Chemistry, 19*, 1968–1977.

Grasdalen, H., & Smidsrød, O. (1987). Gelation of gellan gum. *Carbohydrate Polymers, 7*, 371–393.

He, Y., Yang, F., Zhao, H., Gao, Q., Xia, B., & Fu, J. (2016). Research on the printability of hydrogels in 3D bioprinting. *Scientific Reports, 6*, 29977.

Hyun, K., Kim, S. H., Ahn, K. H., & Lee, S. J. (2002). Large amplitude oscillatory shear as a way to classify the complex fluids. *Journal of Non-Newtonian Fluid Mechanics, 107*, 51–65.

Karvinen, J., Joki, T., Ylä-Outinen, L., Koivisto, J. T., Narkilahti, S., & Kellomäki, M. (2018). Soft hydrazone crosslinked hyaluronan- and alginate-based hydrogels as 3D supportive matrices for human pluripotent stem cell-derived neuronal cells. *Reactive and Functional Polymers, 124*, 29–39.

Kirchmajer D. M., Steinhoff B., Warren H., Clark R., & in het Panhuis M. (2014). Enhanced gelation properties of purified gellan gum. Carbohydrate Research 388, 125–129.

Kocen, R., Gasik, M., Gantar, A., & Novak, S. (2017). Viscoelastic behaviour of hydrogel-based composites for tissue engineering under mechanical load. *Biomedical Materials (Bristol), 12*, Article 025004.

Koivisto, J. T., Gering, C., Karvinen, J., Maria Cherian, R., Belay, B., Hyttinen, J., … Parraga, J. (2019). Mechanically biomimetic gelatin–gellan gum hydrogels for 3D culture of beating human cardiomyocytes. *ACS Applied Materials & Interfaces, 11*, 20589–20602.

Koivisto, J. T., Joki, T., Parraga, J. E., Pääkkönen, R., Ylä-Outinen, L., Salonen, L., … Kellomäki, M. (2017). Bioamine-crosslinked gellan gum hydrogel for neural tissue engineering. *Biomedical Materials, 12*, Article 025014.

Kumar, S., Kaur, P., Bernela, M., Rani, R., & Thakur, R. (2016). Ketoconazole encapsulated in chitosan-gellan gum nanocomplexes exhibits prolonged antifungal activity. *International Journal of Biological Macromolecules, 93*, 988–994.

López-Cebral, R., Paolicelli, P., Romero-Caamaño, V., Seijo, B., Casadei, M. A., & Sanchez, A. (2013). Spermidine-cross-linked hydrogels as novel potential platforms for pharmaceutical applications. *Journal of Pharmaceutical Sciences, 102*, 2632–2643.

Morris, E. R., Nishinari, K., & Rinaudo, M. (2012). Gelation of gellan – A review. *Food Hydrocolloids, 28*, 373–411.

Nakamura, K., Shinoda, E., & Tokita, M. (2001). The influence of compression velocity on strength and structure for gellan gels. *Food Hydrocolloids, 15*, 247–252.

Oliveira, J. T., Martins, L., Picciochi, R., Malafaya, P. B., Sousa, R. A., Neves, N. M., … Reis, R. L. (2010). Gellan gum: A new biomaterial for cartilage tissue engineering applications. *J. Biomed. Mater. Res. Part A, 93A*, 852–863.

Paxton, N., Smolan, W., Böck, T., Melchels, F., Groll, J., & Jungst, T. (2017). Proposal to assess printability of bioinks for extrusion-based bioprinting and evaluation of rheological properties governing bioprintability. *Biofabrication, 9*, Article 044107.

Rasheed, A., Azizi, L., Turkki, P., Janka, M., Hytönen, V. P., & Tuukkanen, S. (2020). *Extrusion-based bioprinting of multilayered nanocellulose constructs for cell cultivation using in situ freezing and preprint CaCl2 cross-linking*. ACS Omega.

Stevens, L. R., Gilmore, J., Wallace, G. G., & M. in het Panhuis, G. G. (2016). Tissue engineering with gellan gum. *Biomaterials Science, 4*, 1276–1290.

Wang, J.-Y., & Casero, R. A., Jr. (2006). *Polyamine structure and synthetic analogs*. 999 Riverview Drive, Suite 208. Totowa, New Jersey 07512: 2006 Humana Press Inc.

Wang, Z. (2010). Malaprade Reaction. In Z. Wang (Ed.), *Comprehensive organic name reactions and reagents* (pp. 1807–1810). American Cancer Society.

Zuidema, J. M., Rivet, C. J., Gilbert, R. J., & Morrison, F. A. (2014). A protocol for rheological characterization of hydrogels for tissue engineering strategies. *Journal of Biomedical Materials Research Part B: Applied Biomaterials, 102*, 1063–1073.